

## Electrochemical Properties of $0.6\text{Li}_2\text{MnO}_3 \cdot 0.4\text{Li}(\text{Ni}_{0.8}\text{Co}_{0.15}\text{Al}_{0.05})\text{O}_2$ Composite Nanopowders Prepared by Spray Pyrolysis

Yong Seung Jang<sup>1</sup>, Jung Hyun Kim<sup>1</sup>, Jung-Kul Lee<sup>1</sup>, Byung Kyu Park<sup>2</sup>, Yun Chan Kang<sup>1,\*</sup>

<sup>1</sup>Department of Chemical Engineering, Konkuk University, 1 Hwayang-dong, Gwangjin-gu, Seoul 143-701, Korea

<sup>2</sup>Suncheon Center, Korean Basic Science Institute, Suncheon 540-742, South Korea

\*E-mail: [yckang@konkuk.ac.kr](mailto:yckang@konkuk.ac.kr)

Received: 22 September 2012 / Accepted: 18 October 2012 / Published: 1 December 2012

---

Nano-sized composite cathode powders [ $0.6\text{Li}_2\text{MnO}_3 \cdot 0.4\text{Li}(\text{Ni}_{0.8}\text{Co}_{0.15}\text{Al}_{0.05})\text{O}_2$ ] are prepared by a scalable spray pyrolysis process. The addition of an organic additive into the spray solution is a key factor for the large production of nano-sized composite cathode powders. After post-treatment at high temperatures and a simple milling process, the composite powders prepared from a spray solution with citric acid and ethylene glycol are the size of nanometers. Mean sizes of the powders after post-treatment at 600 and 900°C are 20 and 200 nm, respectively. An ICP analysis determined that the mole ratio of Li/(Ni + Mn + Co) in the powders post-treated at 900°C, is 1.3. The initial charge capacities of the powders post-treated at 600, 700, 800, and 900°C are 357, 341, 338, and 294 mAh g<sup>-1</sup>. Their initial discharge capacities are 218, 233, 231, and 240 mAh g<sup>-1</sup>. The composite powders post-treated at 900°C have the highest Coulombic efficiency. The discharge capacity of the composite powders post-treated at 900°C decreases from 240 to 229 mAh g<sup>-1</sup> by the 30<sup>th</sup> cycles, in which the capacity retention is 95.4%.

---

**Keywords:** cathode materials, lithium battery, spray pyrolysis, lithium rich, composite material

### 1. INTRODUCTION

Ni-rich cathode materials,  $\text{Li}(\text{Ni}_{0.8}\text{Co}_{0.15}\text{Al}_{0.05})\text{O}_2$  (NCA), have been considered as candidates for high energy lithium ion batteries [1,2]. Layered  $\text{LiNiO}_2$  is a promising cathode material for use in lithium secondary batteries due to its large capacity and low cost [3-8]. However, its high capacity fading and low thermal stability have inhibited its commercialization. Partial substitutions for nickel by transition or non-transition metals are expected to improve its capacity fading upon cycling [1,9-13].

Li-rich Li-Ni-Co oxide compounds have mixed-layered crystal structures of the form  $\text{Li}_2\text{MnO}_3\text{-Li}(\text{Ni}_{1-x}\text{Co}_x)\text{O}_2$  [14-20].  $\text{Li}_2\text{MnO}_3$  stabilizes the electrode structure and enhances the discharge capacity of the  $\text{Li}(\text{Ni}_{1-x}\text{Co}_x)\text{O}_2$  cathode materials. However, the electrochemical and physical properties of Li-rich NCA oxide compounds have not been studied sufficiently.

Spray pyrolysis, one of the gas-phase reaction methods, was developed as a simple and scalable process for the large production of nano-sized cathode powders [21-23]. The nano-sized cathode powders have high power density because they can quickly diffuse  $\text{Li}^+$  ions in the materials at high current densities [24]. However, nano-sized Li-rich cathode powders were scarcely studied in the spray pyrolysis process.

In this study, nano-sized  $0.6\text{Li}_2\text{MnO}_3\cdot 0.4\text{Li}(\text{Ni}_{0.8}\text{Co}_{0.15}\text{Al}_{0.05})\text{O}_2$  composite cathode powders were prepared by a scalable spray pyrolysis process. A key factor in the large production of nano-sized composite cathode powders in the spray pyrolysis process was the addition of an organic additive in the spray solution.

## 2. EXPERIMENTAL

The precursor powders for  $0.6\text{Li}_2\text{MnO}_3\cdot 0.4\text{Li}(\text{Ni}_{0.8}\text{Co}_{0.15}\text{Al}_{0.05})\text{O}_2$  composite powders were prepared using ultrasonic spray pyrolysis. The system consists of ultrasonic spray generator with six vibrators, quartz reactor and Teflon bag filter for powder collection. The inner diameter and the length of the quartz reactor were 50 mm and 1.2 m, respectively. The reactor temperature was maintained at  $900^\circ\text{C}$ . The flow rate of the air used as the carrier gas was fixed at  $40\text{ L min}^{-1}$ . The residence time of the droplet or powders inside the hot wall reactor was 3.5 s. The precursor powders prepared using spray pyrolysis were post-treated at temperatures between 600 and  $900^\circ\text{C}$  for 3 h in oxygen atmosphere. The precursor solutions were prepared by dissolving  $\text{LiNO}_3$  (Junsei, 98%),  $\text{Ni}(\text{NO}_3)_2\cdot 6\text{H}_2\text{O}$  (Junsei, 98%),  $\text{Mn}(\text{NO}_3)_2\cdot 6\text{H}_2\text{O}$  (Junsei, 97%),  $\text{Co}(\text{NO}_3)_2\cdot 6\text{H}_2\text{O}$  (Junsei, 98%) and  $\text{Al}(\text{NO}_3)_3\cdot 9\text{H}_2\text{O}$  (Aldrich, 98%) in distilled water. The Li component added to the spray solution was in excess of 3 wt% of the stoichiometric amount, to facilitate the formation of composite powders. The concentration of the spray solution was 0.5 M. The concentrations of citric acid (CA) and ethylene glycol (EG) used as chelating agents to facilitate the formation of hollow particles were each 0.2 M.

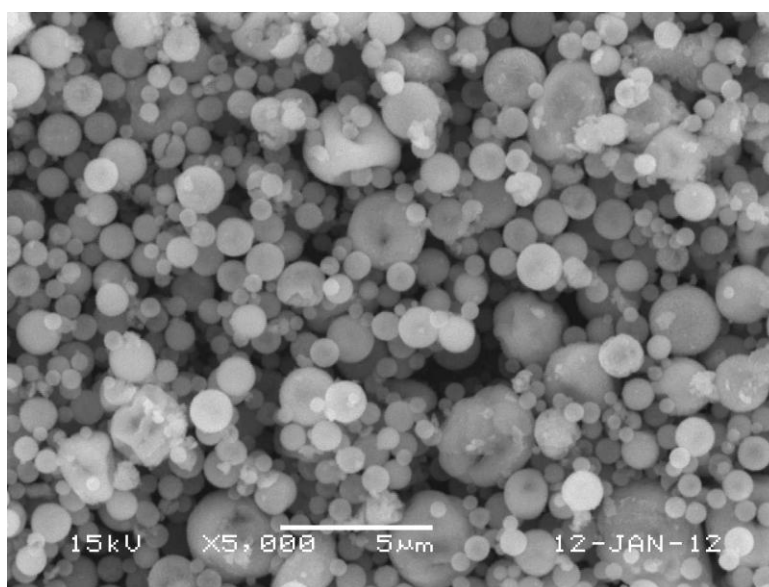
The crystal structures of the prepared cathode powders were investigated using X-ray diffractometry (XRD, X'pert PRO MPD) with  $\text{Cu K}\alpha$  radiation ( $\lambda = 1.5418\text{ \AA}$ ) at the Korea Basic Science Institute (Daegu). The morphological characteristics were investigated using scanning electron microscopy (SEM, JEOL JSM-6060) and high-resolution transmission electron microscopy (TEM, JEOL JEOL-2100F) at 200 kV. The elemental compositions of the powders were investigated using an inductively coupled plasma-optical emission spectrometer (ICP-OES, Thermo elemental, ICAP 6000).

Each cathode electrode was made of 80 wt% active material, 10 wt% carbon black (Super-P) as a conductive material, and 10 wt% polytetrafluoroethylene (PTFE) binder with a few drops of alcohol. All the cathode electrodes were dried at  $120^\circ\text{C}$  for 24 h under vacuum. Li metal and a microporous polypropylene film were used as the anode electrode and the separator, respectively. The electrolyte solution was 1 M  $\text{LiPF}_6$  in a 1:1 mixture by volume of ethylene carbonate/dimethyl carbonate

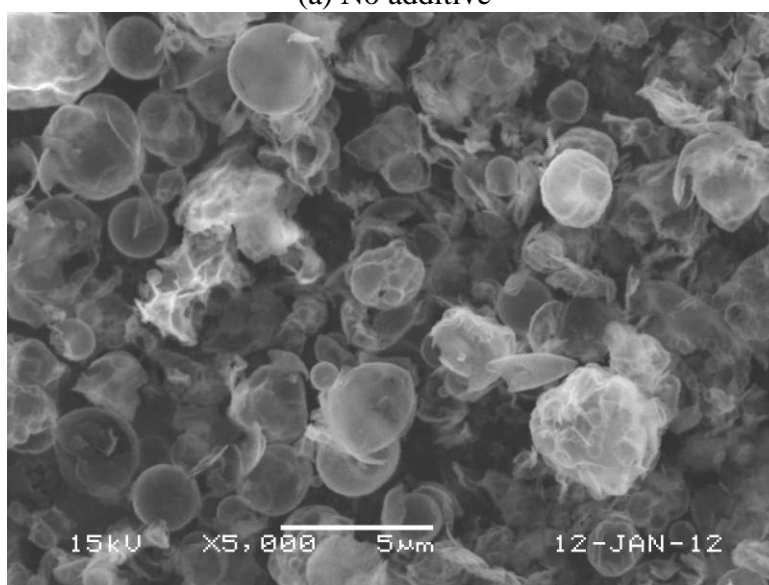
(EC/DMC). The cells were assembled in a glove-box filled with pure argon. The charge/discharge characteristics of the samples were measured through cycling in the 2.0–4.8 V potential range at a constant current density of  $20 \text{ mA g}^{-1}$  with a coin cell (2032 type).

### 3. RESULTS AND DISCUSSION

The morphologies of the precursor powders prepared by spray pyrolysis from the spray solutions with and without organic additives are shown in Fig. 1.

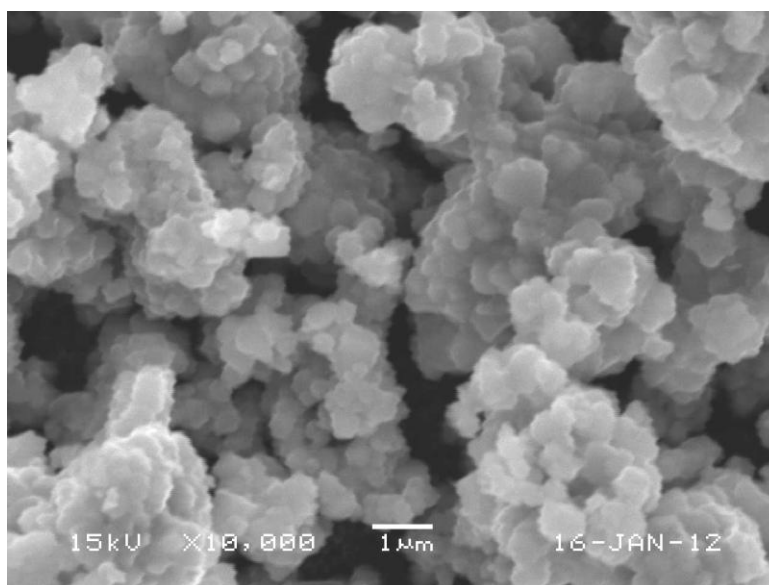


(a) No additive

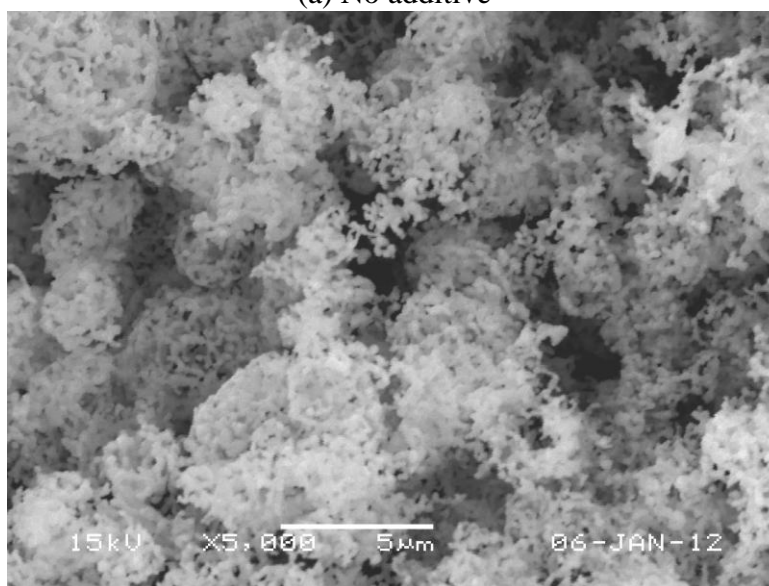


(b) CA&EG

**Figure 1.** SEM images of the precursor powders prepared by spray pyrolysis from the spray solutions with and without organic materials.



(a) No additive



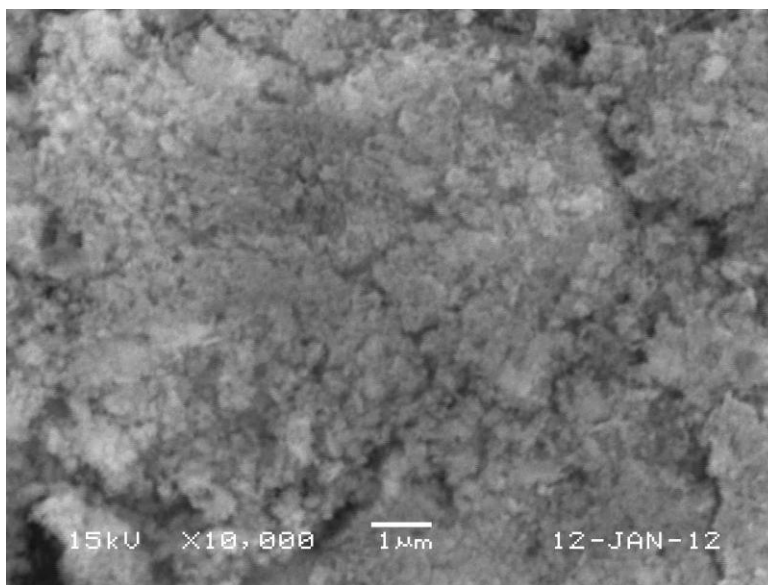
(b) CA&amp;EG

**Figure 2.** SEM images of the composite cathode powders post-treated at 800°C.

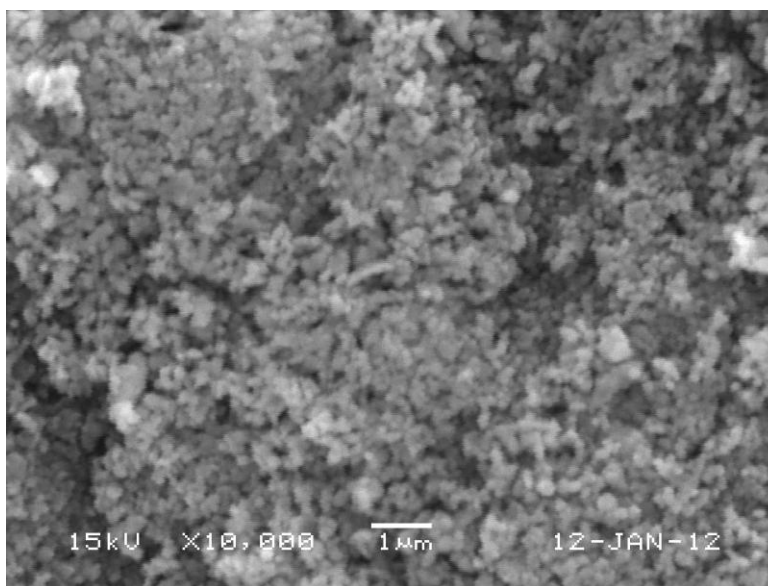
The precursor powders prepared from the spray solution without organic additives had fine sizes, spherical shapes, and dense structures. However, the precursor powders prepared from the spray solution with citric acid and ethylene glycol were large and hollow. They had thin wall structures. The morphologies of the powders prepared by spray pyrolysis were affected by the preparation conditions as well as the types of the spray solutions. In this study, the precursor powders with hollow and thin wall structures were prepared from the spray solution with metal chelates under severe preparation conditions. The types of organic additives and the concentrations dissolved into the spray solution were optimized to prepare the precursor powders.

The morphologies of the  $0.6\text{Li}_2\text{MnO}_3 \cdot 0.4\text{Li}(\text{Ni}_{0.8}\text{Co}_{0.15}\text{Al}_{0.05})\text{O}_2$  composite powders post-treated at 800°C are shown in Fig. 2. The composite powders prepared from the spray solution without

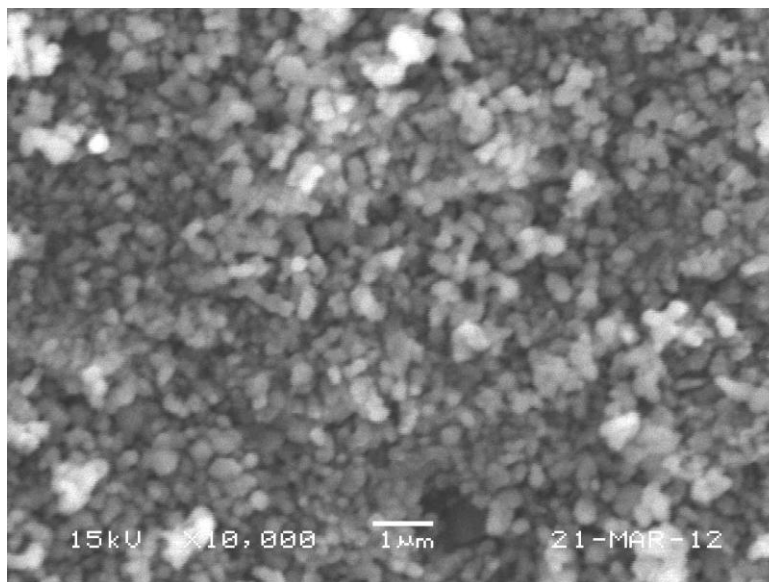
organic additives had irregular shapes and an aggregated morphology. The complete decomposition of the metal salts did not occur because of the short residence time of the powders inside the hot wall reactor. The spherical morphology of the precursor powders disappeared during the decomposition and crystallization processes at 800°C. However, the composite powders prepared from the spray solution with organic additives had porous and a slightly aggregated morphology of the nanometer-sized primary particles. The hollow structure of the precursor powders minimized the particle growth and the aggregation between the powders.



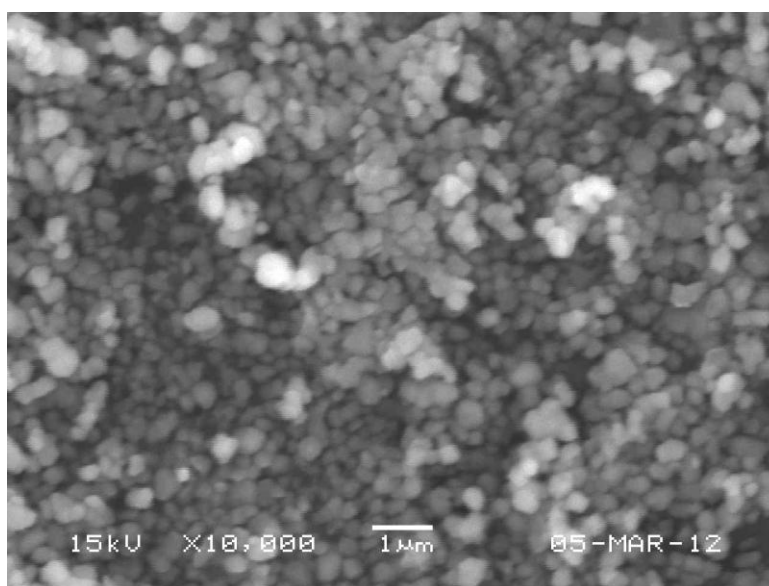
(a) 600°C



(b) 700°C



(c) 800°C



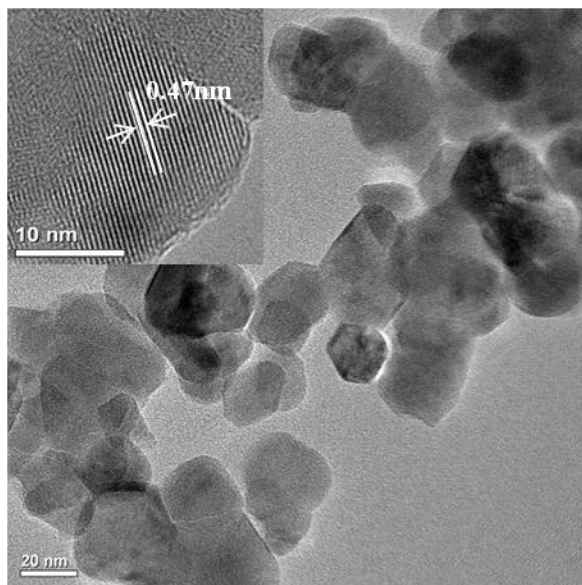
(d) 900°C

**Figure 3.** SEM images of the composite cathode powder post-treated at various temperatures.

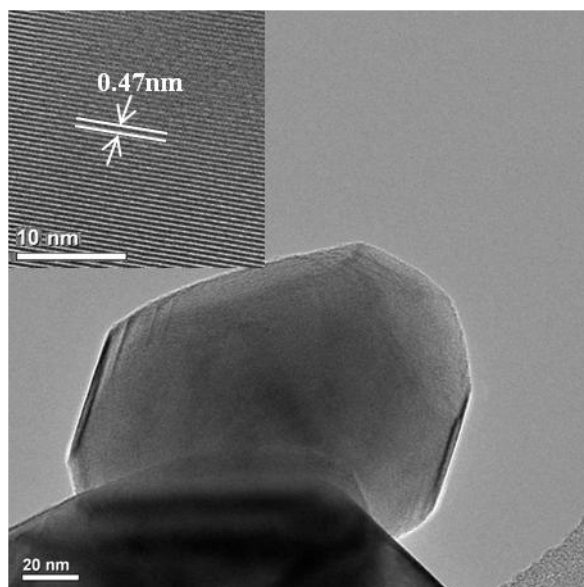
The  $0.6\text{Li}_2\text{MnO}_3 \cdot 0.4\text{Li}(\text{Ni}_{0.8}\text{Co}_{0.15}\text{Al}_{0.05})\text{O}_2$  composite powders prepared from the spray solution with citric acid and ethylene glycol turned into the nano-sized powders after a simple milling process. Figs. 3 and 4 show the morphologies of the composite powders post-treated at temperatures between 600 and 900°C. The post-treated composite powders were milled by hand using an agate mortar. The composite powders had slightly aggregated structures and nanometer sizes irrespective of the post-treatment temperatures. The spherical morphologies of the precursor powders completely disappeared after post-treatment at high temperatures and a simple milling process. The mean sizes of the composite powders increased as the post-treatment temperatures increased. The mean sizes of the

composite powders post-treated at 600 and 900°C measured from the TEM images were 20 and 200 nm, respectively.

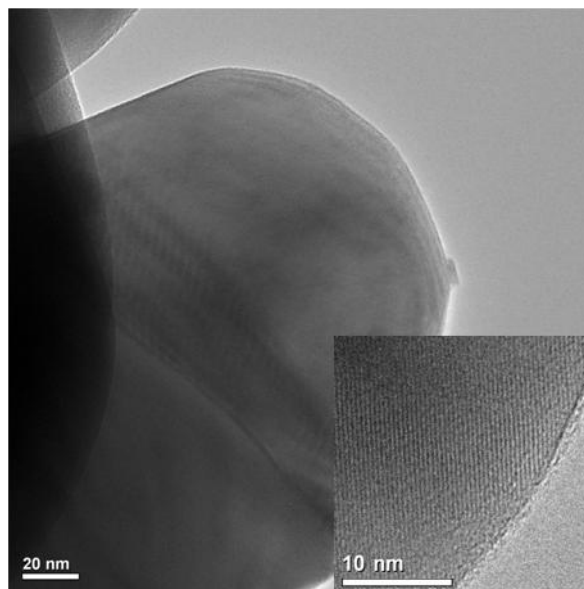
When two solid phases are mixed, each phase prevents the crystal growth of the other phase. Therefore, the composite powders obtained from the precursor powders with hollow and thin wall structures had fine sizes, even at a high post-treatment temperature of 900°C. The BET surface areas of the composite powders post-treated at 600, 700, 800, and 900°C were 18.2, 9.4, 4.7, and 4.1 m<sup>2</sup> g<sup>-1</sup>, respectively. The composite powders had polyhedral structures with clear crystal fringes. High-resolution TEM images exhibited clear lattice fringes with a separation of 0.47 nm.



(a) 600°C



(b) 800°C



(c) 900°C

Figure 4. TEM images of the composite cathode powder post-treated at various temperatures.

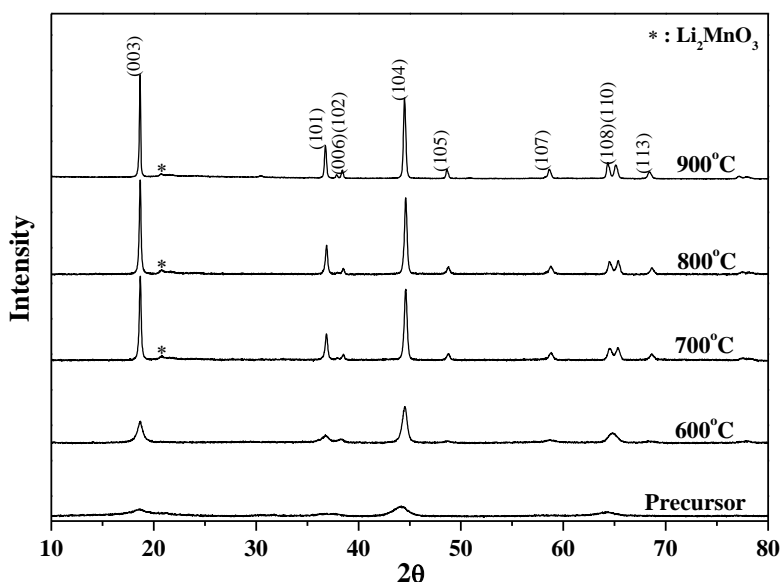
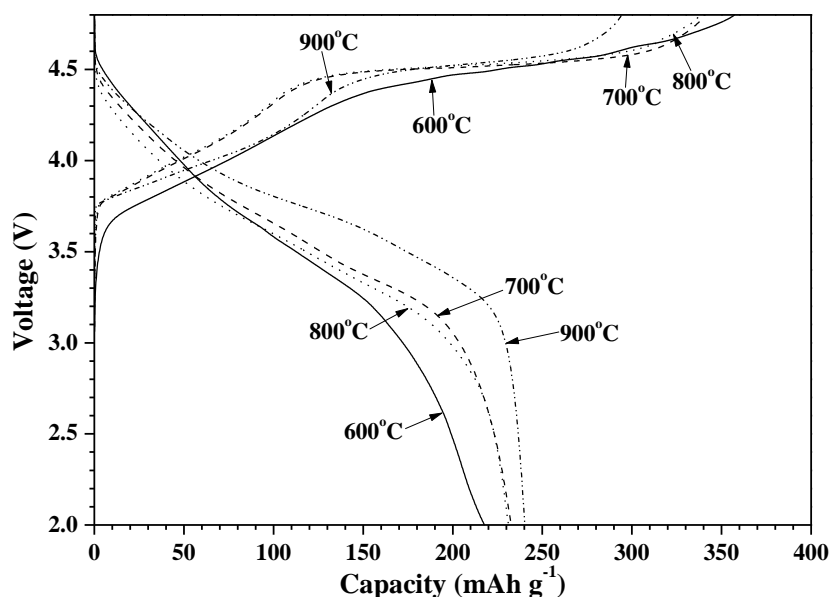


Figure 5. XRD patterns of precursor and composite cathode powders post-treated at various temperatures.

Fig. 5 shows the XRD patterns of the composite powders prepared from the spray solutions with citric acid and ethylene glycol. The XRD patterns of the precursor powders also had crystalline structure even with short residence times of the powders inside the hot wall reactor. Decomposition of the metal salts occurred to form the oxide cathode powders. Sudden heat evolution occurring from the decomposition of organic additives promoted the conversion of metal salts into metal oxide. The XRD

patterns of the samples post-treated at temperatures above 700°C had a peak near 21°, which was attributed to the super lattice structure of  $\text{Li}_2\text{MnO}_3$  [25-27]. The post-treated powders had a mixed-layer crystal structure comprising  $\text{Li}_2\text{MnO}_3$  and  $\text{Li}(\text{Ni}_{0.8}\text{Co}_{0.15}\text{Al}_{0.05})\text{O}_2$  phases, thus forming a composite compound [28,29].

The ordering of the material structure could be estimated from the  $I_{(003)}/I_{(104)}$  intensity ratios and the degrees of the (006)/(102) and (108)/(110) peak splittings [30-34]. The  $I_{(003)}/I_{(104)}$  peak intensity ratios are more than 1 in the samples post-treated at temperatures above 700°C. The (006)/(102) and (108)/(110) peaks are clearly split in the samples post-treated at temperatures above 700°C. As the post-treatment temperatures increased up to 900°C, the sharpness and intensity of the XRD patterns of the composite powders increased. These results indicate that the mean crystallite size of the composite powders increased as the post-treatment temperature increased. The mole ratio of  $\text{Li}/(\text{Ni} + \text{Mn} + \text{Co})$  in the composite powders post-treated at 800°C, as determined by ICP analysis, was 1.3.



**Figure 6.** Initial charge/discharge curves of the composite cathode powders post-treated at various temperatures.

Fig. 6 shows the initial charge/discharge curves of the  $0.6\text{Li}_2\text{MnO}_3 \cdot 0.4\text{Li}(\text{Ni}_{0.8}\text{Co}_{0.15}\text{Al}_{0.05})\text{O}_2$  composite powders post-treated at various temperatures cycled between 2.0 and 4.8 V at room temperature and at a constant current density of  $20 \text{ mA g}^{-1}$ . The composite powders post-treated at 700 and 800°C had similar charge and discharge curves. The composite cathode powders post-treated at 700 and 800°C had similar initial charge capacities by removal of lithium from the  $\text{Li}(\text{Ni}_{0.8}\text{Co}_{0.15}\text{Al}_{0.05})\text{O}_2$  component. They were shown by the smoothly sloping voltage profile below 4.5 V, and by removal of  $\text{Li}_2\text{O}$  from the  $\text{Li}_2\text{MnO}_3$  component, which was shown by voltage plateau above 4.5 V [18-20, 28,29]. The clear voltage plateau above 4.5 V was not observed in the initial

charge curve of the cathode powders post-treated at 600°C. The layered  $\text{Li}_2\text{MnO}_3$  phase was not well formed at a low post-treatment temperature of 600°C as shown by the XRD pattern in Fig. 5. The initial charge curve of the composite powders post-treated at 900°C could also be divided into two main parts. However, the charge capacity of the composite powders post-treated at 900°C by removal of  $\text{Li}_2\text{O}$  from the  $\text{Li}_2\text{MnO}_3$  component, shown by a voltage plateau above 4.5 V, was smaller than those of the composite powders post-treated at 700 and 800°C. For cathode powders post-treated at 600, 700, 800, and 900°C, the initial charge capacities were 357, 341, 338, and 294  $\text{mAh g}^{-1}$ . The initial discharge capacities were 218, 233, 231, and 240  $\text{mAh g}^{-1}$ . The cathode powders post-treated at 600°C had the lowest Coulombic efficiency because of their poor crystallinity and phase inhomogeneity. The composite powders post-treated at 900°C had the highest Coulombic efficiency because a small amount of  $\text{Li}_2\text{O}$  was removed from the  $\text{Li}_2\text{MnO}_3$  component in an initial charge stage. The first cycles of the composite powders post-treated at 700 and 800°C had low Coulombic efficiencies. The high first-cycle irreversible capacity loss of the cell is typical of a "layered-layered" composite electrode [35,36].

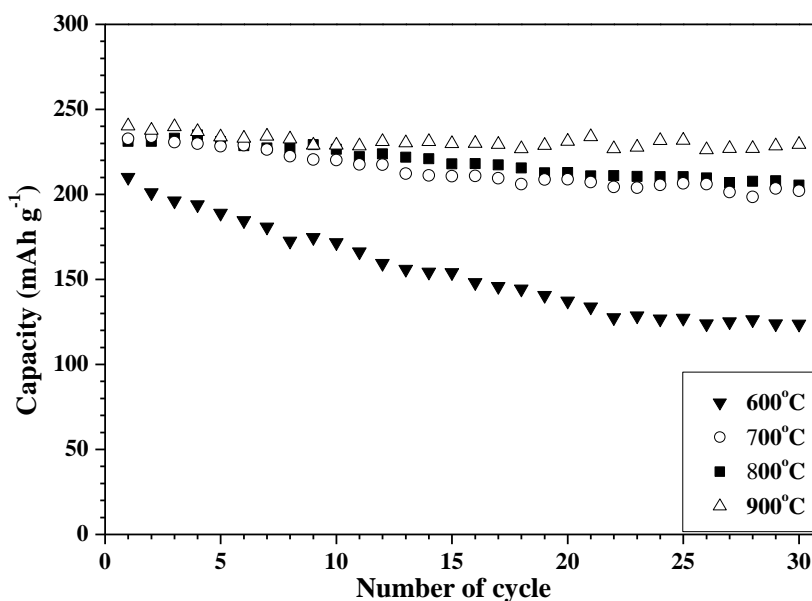


**Figure 7.** Cycle properties of the composite cathode powders post-treated at various temperatures.

Fig. 7 shows the cycle properties of the composite powders post-treated at various temperatures cycled between 2.0 and 4.8 V at room temperature and at a constant current density of 20  $\text{mA g}^{-1}$ . The cathode powders post-treated at a low temperature of 600°C had poor cycle properties. The cycle properties of the composite powders improved as the post-treatment temperatures of the powders increased. The discharge capacity of the composite powders post-treated at 900°C decreased from 240  $\text{mAh g}^{-1}$  to 229  $\text{mAh g}^{-1}$  by the 30<sup>th</sup> cycles, in which the capacity retention was 95.4%. However, the capacity retentions of the composite powders post-treated at 700 and 800°C were 86.9 and 88.7% after 30<sup>th</sup> cycles.

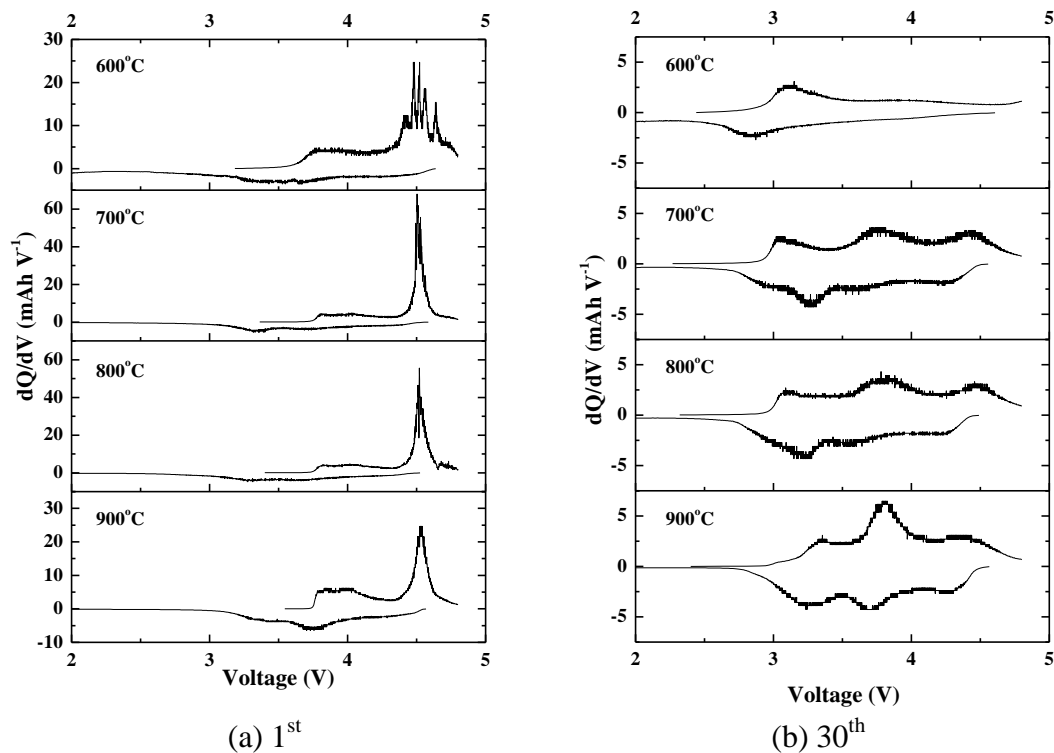


**Figure 8.**  $dQ/dV$  curves for composite cathode powders post-treated at various temperatures for the 1<sup>st</sup> and 30<sup>th</sup> cycles.

Fig. 8 shows the differential capacity vs. voltage ( $dQ/dV$ ) curves for cathode materials post-treated at various temperatures for the 1<sup>st</sup> and 30<sup>th</sup> cycles. The first charge curve of the composite powders had two distinct oxidation peaks at around 3.8 and 4.6 V. The peak at around 3.8 V was due to the oxidation of  $\text{Ni}^{2+}$  to  $\text{Ni}^{4+}$ . The peak at around 4.6 V was due to the irreversible reaction involving the removal of lithium and oxygen as  $\text{Li}_2\text{O}$  from  $\text{Li}_2\text{MnO}_3$  [18-20,28]. The first discharge curve had two distinct reduction peaks between 3.5 and 4.5 V, corresponding to the reduction of  $\text{Ni}^{4+}$  to  $\text{Ni}^{2+}$  [28]. No redox-reaction peaks below 3.5 V were found in the first charge curve, indicating that Mn is present as  $\text{Mn}^{4+}$  in the sample. On the other hand, a reduction peak ascribed to the reduction of  $\text{Mn}^{4+}$  to  $\text{Mn}^{3+}$  was observed below 3.5 V in the  $dQ/dV$  curves for the 30<sup>th</sup> cycles of the cathode powders. The inactive  $\text{MnO}_2$  formed by the leaching of  $\text{Li}_2\text{O}$  from the  $\text{Li}_2\text{MnO}_3$  component in the first charging process was activated to form layered  $\text{LiMnO}_2$  cathode material in the following discharge processes [37]. The reduction peaks of the Mn ions clearly shift to the low-voltage regions in the  $dQ/dV$  curves for the 30<sup>th</sup> cycles while decreasing the post-treatment temperatures of the cathode powders. This indicated that phase transition from the layered composite cathode to the  $\text{LiMn}_2\text{O}_4$  spinel phase, which is unstable when cycling at high operating voltages, occurred. The shift of the reduction peak of the Mn ions to the low-voltage region in the  $dQ/dV$  curve for the 30<sup>th</sup> cycle of the composite powders post-treated at 900°C did not occur. Thus, the stabilization effect of the  $\text{Li}_2\text{MnO}_3$  phase improved the cycle properties of the composite cathode powders post-treated at 900°C.

#### 4. CONCLUSIONS

Nano-sized  $0.6\text{Li}_2\text{MnO}_3 \cdot 0.4\text{Li}(\text{Ni}_{0.8}\text{Co}_{0.15}\text{Al}_{0.05})\text{O}_2$  composite cathode powders are prepared by spray pyrolysis from a spray solution with citric acid and ethylene glycol. The precursor powders with large size, hollow and thin wall structure obtained by spray pyrolysis turn into nano-sized composite cathode powders after post-treatment at temperatures between 600 and 900°C. However, the composite powders prepared from the spray solution without organic additives are large in size and have an aggregated structure. The electrochemical properties of the nano-sized composite powders are affected by the post-treatment temperatures of the powders. The composite powders post-treated at 900°C have the highest initial discharge capacity even though they have the lowest initial charge capacity. The charge capacity of the composite powders post-treated at 900°C by removal of  $\text{Li}_2\text{O}$  from the  $\text{Li}_2\text{MnO}_3$  component, shown by voltage plateau above 4.5 V, is smaller than those of the composite powders post-treated at 700 and 800°C. The stabilization effect of the  $\text{Li}_2\text{MnO}_3$  phase improves the cycle properties of the composite cathode powders post-treated at 900°C.

#### ACKNOWLEDGEMENT

This work was supported by the National Research Foundation of Korea(NRF) grant funded by the Korea government(MEST) (No. 2012R1A2A2A02046367). This study was supported by the Converging Research Center Program through the National Research Foundation of Korea (NRF) funded by the Ministry of Education, Science and Technology (2011-50210).

#### References

1. T. Ohzuku, A. Ueda, M. Kouguchi, *J. Electrochem. Soc.*, 142 (1995) 4033
2. S.H. Ju, H.C. Jang, Y.C. Kang, *Electrochim. Acta*, 52 (2007) 7286
3. M.G.S.R. Thomas, W.I.F. David, J.B. Goodenough, P. Groves, *Mater. Res. Bull.*, 20 (1985) 1137
4. J.R. Dahn, U. Von Sacken, M.W. Jozkow, H. Al-Janaby, *J. Electrochem. Soc.*, 138 (1991) 2207
5. M. Broussely, F. Perton, J. Labat, R.J. Staniewicz, A. Romero, *J. Power Sources*, 43 (1993) 209
6. T. Ohzuku, A. Ueda, *Solid State Ionics*, 69 (1994) 201
7. M. Broussely, F. Perton, P. Biensan, J.M. Bodet, J. Labat, A. Lecerf, C. Delmas, A. Rougier, J.P. Pérès, *J. Power Sources*, 54 (1995) 109
8. C. Delmas, M. Ménétrier, L. Croguennec, I. Saadoune, A. Rougier, C. Poullierie, G. Prado, M. Grüne, L. Fournès, *Electrochim. Acta*, 45 (1999) 243
9. T. Ohzuku, A. Ueda, M. Nagayama, *J. Electrochem. Soc.*, 140 (1993) 1862
10. J.R. Dahn, E.W. Fuller, M. Obrovac, U. von Sacken, *Solid State Ionics*, 69 (1994) 265
11. H. Arai, S. Okada, Y. Sakurai, J. Yamaki, *Solid State Ionics*, 109 (1998) 295
12. Y. Gao, M.V. Yakobleva, W.B. Ebner, *Electrochem. Solid-state Lett.*, 1 (1998) 117
13. T. boyle, D. Ingersoll, M.A. Rodreguez, C.J. Tafoya, D.G. Doughty, *J. Electrochem. Soc.*, 146 (1999) 1683
14. J.H. Lim, H. Bang, K.S. Lee, K. Amine, Y.K. Sun, *J. Power Sources*, 189 (2009) 571
15. X.J. Guo, Y.X Li, M. Zheng, J.M. Zheng, J. Lie, Z.L. Gong, Y. Yang, *J. Power Sources*, 184 (2008) 414
16. K.M. Shaju, G.V. Subba Rao, B.V.R. Chowdari, *Electrochim. Acta*, 48 (2002) 145
17. J. Wang, Y. Xia, X. Yao, M. Zhang, Y. Zhang, Z. Liu, *Int. J. Electrochem. Sci.*, 6 (2011) 6670
18. J.M. Zheng, X.B. Wu, Y. Yang, *Electrochim. Acta*, 56 (2011) 3071
19. R. Santhanam, B. Rambabu, *Int. J. Electrochem. Sci.*, 4 (2009) 1770
20. C. Gan, H. Zhan, X. Hu, Y. Zhou, *Electrochem. Commun.*, 7 (2005) 1318

21. S.H. Ju, Y.C. Kang, *Ceram. Int.* 35 (2009) 1633
22. Y. N. Ko, J. H. Kim, Y. J. Hong, Y. C. Kang, *Mater. Chem. Phys.*, 131 (2011) 292
23. S.H. Ju, H.Y. Koo, S.K. Hong, E.B. Jo, Y.C. Kang, *J. Power Sources*, 174 (2007) 598
24. K.M. Begam, S.R.S. Prabakaran, *J. Power Sources*, 159 (2006) 319
25. Z. Lu, L.Y. Beaulieu, A. Donaberger, C.L. Thomas, J.R. Dahn, *J. Electrochem. Soc.*, 149 (2002) A778
26. M.M. Thackeray, S.H. Kang, C.S. Johnson, J.T. Vaughey, R. Benedek, S.A. Hackney, *J. Mater. Chem.*, 17 (2007) 3112
27. Z. Lu, Z. Chen, J.R. Dahn, *Chem. Mater.*, 15 (2003) 3214
28. C.S. Johnson, J.S. Kim, C. Lefief, N. Li, J.T. Vaughey, M.M. Thackeray, *Electrochem. Commun.*, 6 (2004) 1085
29. J.S. Kim, C.S. Johnson, J.T. Vaughey, M.M. Thackeray, S.A. Hackney, W. Yoon, C.P. Grey, *Chem. Mater.*, 16 (2004) 1996
30. J. Maruta, H. Yasuda, M. Yamachi, *J. Power Sources*, 90 (2000) 89
31. S.H. Park, K.S. Park, Y.K. Sun, K.S. Nahm, Y.S. Lee, M. Yoshio, *Electrochim. Acta*, 46 (2001) 1215
32. Z.L. Gong, H.S. Liu, X.J. Guo, Z.R. Zhang, Y. Yang, *J. Power Sources*, 136 (2004) 139
33. L. Yu, W. Qiu, F. Lian, J. Huang, X. Kang, *J. Alloys Compd.*, 471 (2009) 317
34. H. Cao, B. Xia, N. Xu, C. Zhang, *J. Alloys Compd.*, 376 (2004) 282
35. Y. Wu, A. Manthiram, *Electrochem. Solid-State Lett.*, 9 (2006) A221
36. J.M. Zheng, Z.R. Zhang, X.B. Wu, Z.X. Dong, Z. Zhu, Y. Yang, *J. Electrochem. Soc.*, 155 (2008) A775
37. Z. Lu, J.R. Dahn, *J. Electrochem. Soc.*, 149 (2002) A815